This article has been accepted for publication in a future issue of this journal, but has not been fully edited. Content may change prior to final publication. Citation information: DOI 10.1109/TAP.2015.2418343, IEEE Transactions on Antennas and Propagation

Spatially Large-Domain and Temporally Entire-Domain Electric-Field Integral Equation Method of Moments for 3-D Scattering Analysis in Time Domain

Nada J. Šekeljić, *Student Member, IEEE*, Milan M. Ilić, *Member, IEEE*, and Branislav M. Notaroš, *Senior Member, IEEE*

***Abstract*—A novel spatially large-domain and temporally entire-domain method of moments (MoM) is proposed for surface integral equation (SIE) modeling of 3-D conducting scatterers in the time domain (TD). The method uses higher order curved Lagrange interpolation generalized quadrilateral geometrical elements, higher order spatial current expansions based on hierarchical divergence-conforming polynomial vector basis functions, and temporal current modeling by means of orthogonal weighted associated Laguerre basis functions. It implements full temporal and spatial Galerkin testing and marching-on-in-degree (MOD) scheme for an iterative solution of the final system of spatially and temporally discretized MoM-TD equations. Numerical examples demonstrate excellent accuracy, efficiency, convergence, and versatility of the new MoM-MOD method. The results also demonstrate very effective large-domain MoM-TD SIE models of scatterers using flat and curved patches of electrical sizes of up to about 1.7 wavelengths at the maximum frequency in the frequency spectrum of the pulse excitation, higher order current expansions of spatial orders from 2 to 8 in conjunction with entire-domain Laguerre temporal bases, and minimal numbers of unknowns.**

***Index Terms*—Electromagnetic analysis, numerical techniques, method of moments, surface integral equations, time domain analysis, higher order modeling, curved parametric elements, polynomial basis functions, scattering, transient response.**

I. Introduction

THE TIME-DOMAIN (TD) surface integral equation (SIE) formulation is an effective approach to transient electromagnetic (EM) analysis of open-region (radiation and scattering) three-dimensional (3-D) structures. TDSIE techniques have two unique advantages as compared to differential equation based numerical approaches, such as the finite element method (FEM), when analyzing homogeneous or piecewise homogeneous radiation and scattering structures in the TD. As SIE based methods, they only require surface discretization of the scatterer and implicitly satisfy radiation boundary condition through Green's functions. As TD methods, they can provide analysis of transient, broadband, and nonlinear phenomena in a single run.

The most explored method in solving TDSIEs is the marching-on-in-time (MOT) method [1]. Several MOT schemes, combined with the method of moments (MoM) Galerkin-type spatial testing, have been developed [2]–[7]. In terms of the numerical properties of proposed and implemented temporal basis functions and their orders, most MOT techniques apply linear approximations of the temporal current expansions [3], [4], [8]–[12]. Higher order Lagrange polynomial temporal basis functions, implemented up to the second order, have been suggested in order to enhance the accuracy of the MOT algorithm [7], [13]–[17].

Novel higher order temporal basis functions derived from Laguerre polynomials are introduced in [18]. These polynomials naturally satisfy the causality condition because they are defined on the interval from zero to infinity (entire-domain temporal basis functions); therefore, they are a desirable choice for transient modeling. By applying the temporal testing procedure in the same fashion as the spatial Galerkin-type testing, and due to the orthogonality of Laguerre polynomials, the temporal variable can be integrated analytically out from the final system of TDSIEs. Instead of the conventional MOT procedure, the final system of equations is solved in marching-on-in-degree (MOD) of temporal basis functions. Like implicit MOT schemes [6], the MOD approach does not have to satisfy the Courant-Friedrich-Levy (CFL) sampling criterion relating the spatial to the temporal discretization. The MOD scheme employing weighted Laguerre polynomials as temporal bases has been implemented within different MoM-SIE formulations in the TD, including the electric field integral equation (EFIE), magnetic field integral equation (MFIE), and combined field integral equation (CFIE) formulations, for transient scattering

Manuscript received June 17, 2014, revised December 7, 2014. This work was supported by the National Science Foundation under grants ECCS-1002385 and ECCS-1307863 and by the Serbian Ministry of Education, Science, and Technology under Grant TR-32005.

N. J. Šekeljić and B. M. Notaroš are with Colorado State University, Department of Electrical and Computer Engineering, Fort Collins, CO 80523-1373 USA (phone: 970-491-3537; fax: 970-491-2249; e-mail: inadasek@engr.colostate.edu, notaros@colostate.edu).

M. M. Ilić is with University of Belgrade, School of Electrical Engineering, 11120 Belgrade, Serbia and with the Colorado State University, Department of Electrical and Computer Engineering, Fort Collins, CO 80523-1373, USA (e-mail: milanilic@etf.rs).

This article has been accepted for publication in a future issue of this journal, but has not been fully edited. Content may change prior to final publication. Citation information: DOI 10.1109/TAP.2015.2418343, IEEE Transactions on Antennas and Propagation

analysis of conducting and dielectric structures [19]–[26]. Compared to the implicit MOT scheme, which results in a sparse system matrix and where the sparsity/stability depends on the size of the time step, the MOD scheme produces a full system matrix independent of the time step/order of the time-variant basis functions. The minimal order of the Laguerre polynomials for the temporal support is defined by the time duration and frequency bandwidth product of an incident wave [19], [21]. Finally, the Laguerre polynomials decay to zero at infinite time, thus the solution cannot become oscillatory for late times.

In terms of the numerical properties of proposed and implemented spatial basis functions and their orders, however, practically all the existing MOT and MOD 3-D MoM-TD SIE simulation tools for EM scattering analysis are low-order or small-domain (subdomain) techniques, with the EM structure being modeled by planar triangular surface elements that are electrically very small and the electric and magnetic currents over the elements are approximated by the first-order spatial basis functions, namely, Rao-Wilton-Glisson (RWG) functions [27]. This results in a very large number of spatial unknowns (unknown current-distribution coefficients) needed to obtain results of satisfactory accuracy, with all the associated problems and large requirements in computational resources. In addition, flat triangular patches do not provide enough flexibility and efficiency in modeling of structures with pronounced curvature.

An alternative approach – constituting the higher order or large-domain (sometimes also referred to as the entire-domain) computational EM [28] – is based on using higher order basis functions defined on large curved geometrical elements (patches) [29], which can greatly reduce the number of unknowns for a given problem and enhance the accuracy and efficiency of the computation. However, this approach seems to have not been fully employed in the MoM-TD SIE analysis yet; namely, almost none of the reported MoM-MOT/MOD TD SIE results and applications in the literature demonstrate actual using and implementation of spatial discretization models with current approximation orders higher than one (higher order modeling). Moreover, for MoM-TD SIE modeling of general structures that may possess arbitrary curvature, it is convenient to have both higher order geometrical flexibility for curvature modeling and higher order current-approximation flexibility for spatial current modeling – in the same method. Also, it is convenient to use hierarchical higher order bases, which allow elements of different orders and sizes combined together in the same model. Notable examples of spatially higher order MoM-MOT TD SIE modeling are the boundary integral equation (BIE) method in the TD using isoparametric curvilinear quadratic approximation of geometry and both spatial and temporal dependence of fields [30], [31] and the higher order Calderon preconditioned EFIE TD solver employing Graglia-Wilton-Peterson (GWP) divergence- and quasi curl-conforming (DQCC) spatial basis functions of up to third order on second-order curvilinear triangular elements [32]. Another example are spatially higher order vector basis functions (up to the second order) in conjunction with band-limited interpolatory functions (BLIFs) for temporal discretization have been introduced in [5]. In addition, none of the works employ large elements (or a combination of large and small elements) in the MoM-TD SIE model (large-domain modeling).

This paper proposes a novel spatially large-domain and temporally entire-domain MoM-TD EFIE method, with full temporal and spatial Galerkin testing, for 3-D transient EM analysis of conducting scatterers based on higher order geometrical modeling and current expansion and MOD scheme. The geometry of the structure is modeled using Lagrange-type interpolation generalized quadrilaterals of arbitrary geometrical-mapping orders and the spatial current distributions over the elements are expanded in terms of hierarchical divergence-conforming polynomial vector basis functions of arbitrarily high current-approximation orders [29]. Note that the quadrilateral elements have been chosen to facilitate surface meshes that can employ very large elements, which is consistent with the large-domain modeling and higher order current expansion paradigm. Triangular elements could be used (with appropriate local parent coordinate systems) but with limited flexibility in terms of large-domain modeling. Time variations of the currents are expressed by orthogonal entire-domain temporal basis functions derived from Laguerre polynomials and the transient response of the scatterer is obtained by an iterative solution of the final system of spatially and temporally discretized MoM-TD EFIE equations in a MOD fashion [26]. It should be noted that the MOD is a particularly suitable choice here since the focus of this paper is on higher order spatial elements. However, MOD has seen limited use in literature because its efficiency may often be considerably weaker than with the methods that use local basis functions in time, e.g., [32].

To the best of our knowledge, this paper presents the first MoM-TD SIE method with very high spatial and temporal expansion orders (the results demonstrate using current expansions of spatial orders from 2 to 8 and geometrical-mapping orders from 1 to 4 in conjunction with using higher order, entire-domain Laguerre polynomial temporal basis functions) and the first set of spatially large-domain MoM-TD SIE modeling examples (the electrical sizes of flat and curved patches in models are up to about 1.7 wavelengths at the maximum frequency in the frequency spectrum of the pulse excitation). The new method is also the first MoM-MOD method with spatially higher order expansions.

Section II of the paper presents development and

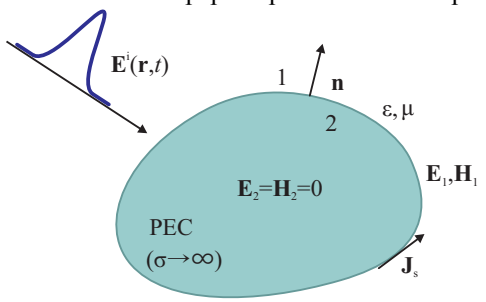

Fig. 1. 3-D PEC scatterer excited by an incident Gaussian pulse – analysis by the MoM-MOD TD EFIE method.

This article has been accepted for publication in a future issue of this journal, but has not been fully edited. Content may change prior to final publication. Citation information: DOI 10.1109/TAP.2015.2418343, IEEE Transactions on Antennas and Propagation

implementation of all major numerical components of the new MoM-MOD technique. In Section III, the technique is validated and its accuracy and efficiency evaluated and discussed in several characteristic examples.

II. Novel MoM-MOD TD EFIE Method

A. EFIE Formulation in TD

Consider a 3-D conducting, nonpenetrable (PEC – perfect electric conductor) body excited by an incident wave (e.g., a Gaussian pulse or its derivative), as shown in Fig. 1. The total tangential electric field (superposition of incident field $\mathbf{E}_\mathrm{i}$ and scattered field $\mathbf{E}$) on the boundary surface S is equal to zero at each time instant,

$$[\mathbf{E}(\mathbf{r},t)]_{\mathrm{tang}} + [\mathbf{E}_\mathrm{i}(\mathbf{r},t)]_{\mathrm{tang}} = 0, \quad \mathbf{r} \in S, \quad (\forall)\, t \geq 0\,. \tag{1}$$

The scattered electric field in the unbounded homogeneous background medium of permittivity ε and permeability μ is expressed in terms of surface electric current density vector $\mathbf{J}_\mathrm{S}$ over S as follows:

$$\mathbf{E}(\mathbf{r},t) = -\frac{\partial \mathbf{A}(\mathbf{r},t)}{\partial t} - \nabla\Phi(\mathbf{r},t)\,. \tag{2}$$

The Lorenz (retarded) potentials are given by

$$\mathbf{A}(\mathbf{r},t) = \frac{\mu}{4\pi}\int_S \frac{\mathbf{J}_\mathrm{S}(\mathbf{r}',t-R/c)}{R}\,\mathrm{d}S\,, \tag{3}$$

$$\Phi(\mathbf{r},t) = \frac{1}{4\pi\,\varepsilon}\int_S \frac{\rho_\mathrm{S}(\mathbf{r}',t-R/c)}{R}\,\mathrm{d}S = -\frac{1}{4\pi\varepsilon}\int_S \int_0^{t-R/c} \frac{\nabla_\mathrm{s}\cdot\mathbf{J}_\mathrm{S}(\mathbf{r}',t')}{R}\,\mathrm{d}t'\mathrm{d}S\,, \tag{4}$$

where $R = |\mathbf{r}-\mathbf{r}'|$ represents the distance between the observation point $\mathbf{r}$ and the source point $\mathbf{r}'$, $\tau = t - R/c$ is the time (delay) that the EM wave travels from the source to the observation point, and c is the intrinsic speed of propagation of the EM wave in the background medium. Note that in (4), the surface charge density ρ_s is related to $\mathbf{J}_\mathrm{S}$ based on the continuity equation, $\nabla_\mathrm{s}\cdot\mathbf{J}_\mathrm{S} = -\partial\rho_\mathrm{S}/\partial t$. Having in mind the integral expressions for scattered electric field $\mathbf{E}$ in (2)–(4), (1) represents the TD EFIE for $\mathbf{J}_\mathrm{S}$ as unknown, which is discretized and solved using the MoM with Galerkin testing in space-time in conjunction with the MOD scheme [24], [25].

B. Geometrical Modeling Using Higher Order Quadrilateral Surface Elements

The geometry of the structure in Fig. 1 is modeled by means of generalized curved quadrilateral patches shown in Fig. 2 and analytically described as [29]

$$\mathbf{r}(u,v) = \sum_{k=0}^{K_u}\sum_{l=0}^{K_v} \mathbf{r}_{kl}\,\Lambda_k^{K_u}(u)\,\Lambda_l^{K_v}(v)\,,\ -1 \leq u,v \leq 1\,, \tag{5}$$

where K_u and K_v (K_u, $K_v \geq 1$) are geometrical orders of the element along u and v parametric coordinates, respectively (note that the orders do not need to be the same within an element), $\mathbf{r}_{kl}$ are constant vector coefficients related to position vectors of the interpolation nodes, see Fig.2, $\Lambda(u)$ represent Lagrange interpolation polynomials in the u coordinate,

$$\Lambda_k^{K_u}(u) = \prod_{\substack{j=0 \\ j\neq k}}^{K_u} \frac{u-u_j}{u_k-u_j}\,, \tag{6}$$

with the nodes defined as $u_j = (2j-K_u)/K_u$, $j = 0,1,\ldots,K_u$, and similarly for $\Lambda(v)$. Usually, the equidistant distribution of interpolation nodes along each coordinate in parametric space is used. Of course, the use of specific nonequidistant node distribution, which would provide additional modeling flexibility and accuracy in some applications, is possible as well. Note that the 3-D generalization of the quadrilateral in Fig. 2 is used in the higher order FEM-TD method [33].

C. Higher Order Temporal and Spatial Basis Functions

In the novel MoM-TD EFIE method, the time-variant electric current density and the accompanying surface charge density over every generalized quadrilateral in the model are expanded using temporal and spatial higher order basis functions as follows:

$$\mathbf{J}_\mathrm{S}(\mathbf{r},t) = \frac{\partial \mathbf{h}(\mathbf{r},t)}{\partial t}\,,\ \rho_\mathrm{S}(\mathbf{r},t) = -\nabla\cdot\mathbf{h}(\mathbf{r},t)\,, \tag{7}$$

$$\mathbf{h}(u,v,t) = \sum_{i=0}^{N_u}\sum_{j=0}^{N_v-1} h_{uij}(t)\,\mathbf{f}_{uij}(u,v) + \sum_{i=0}^{N_u-1}\sum_{j=0}^{N_v} h_{vij}(t)\,\mathbf{f}_{vij}(u,v) \tag{8}$$

where $\mathbf{h}$ is the Hertz vector introduced as the actual unknown in the MoM solution procedure in order to avoid temporal integration in (4) [34], [21], and u and v are local parametric

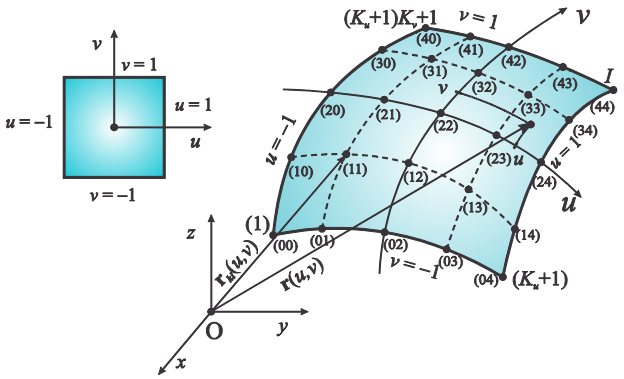

Fig. 2. Generalized curved parametric quadrilateral MoM-SIE patch defined by (5), with the square parent domain.

This article has been accepted for publication in a future issue of this journal, but has not been fully edited. Content may change prior to final publication. Citation information: DOI 10.1109/TAP.2015.2418343, IEEE Transactions on Antennas and Propagation

coordinates of an element (SIE patch) in the model [see Eq. (5)]. Unknown time-dependent coefficients in (8) associated with the *u*-component of the Hertz vector h_{uij} are expanded using a linear combination of the three associated Laguerre functions with successive orders,

$$h_{uij}(t)=\sum_{q=0}^{M} h_{uij,q}\left(\Psi_q(st)-2\Psi_{q+1}(st)+\Psi_{q+2}(st)\right) \tag{9}$$

(time-dependent coefficients associated with *v*-component of the Hertz vector h_{vij} can be expanded in a similar fashion). Here, M is the order of temporal basis functions, s is the scaling factor which controls the accuracy of the temporal support, $h_{uij,q}$ are unknown constant coefficients, $\Psi_q(st)=\mathrm{e}^{-st/2}L_q(st)$, $t\ge 0$, are associated Laguerre temporal basis functions, and $L_q(st)$ are Laguerre polynomials of order q and argument $x = st$, defined as

$$L_q(x)=\frac{\mathrm{e}^x}{q!}\frac{\mathrm{d}^q}{\mathrm{d}x^q}(x^q\mathrm{e}^{-x}),\quad q\ge 0, x\ge 0\,. \tag{10}$$

These polynomials satisfy the following recursive relation:

$$\begin{aligned} &L_0(x)=1,\ L_1(x)=1-x,\\ &L_q(x)=\frac{1}{q}((2q-1-x)L_{q-1}(x)-(q-1)L_{q-2}),\ q\ge 2. \end{aligned} \tag{11}$$

Linear combination of weighted Laguerre polynomials, (9), is suggested in [24], [26] in order to improve the computational efficiency as compared to the conventional MOD method where the time-dependent part of the Hertz vector is expanded only by a single associated Laguerre function set $\Psi_q(st)$ [21], [23], [25]. The Laguerre polynomials have excellent causality, orthogonally, recursive-computation, and convergence properties [24], and are extremely convenient for the purpose of temporal expansions in the large-domain MoM-TD EFIE method. Functions $\mathbf{f}$ in (8) are higher order hierarchical-type divergence-conforming spatial basis functions defined on each generalized quadrilateral patch (see Fig. 2). For the local *u*- and *v*-components of the Hertz vector, they are given by [29]

$$\begin{aligned} &\mathbf{f}_{uij}(u,v)=\frac{P_i(u)v^j}{\mathfrak{I}(u,v)}\mathbf{a}_u(u,v),\\ &\mathbf{f}_{vij}(u,v)=\frac{u^iP_j(v)}{\mathfrak{I}(u,v)}\mathbf{a}_v(u,v),\\ &P_i(u)=\begin{cases}1-u, & i=0\\ u+1, & i=1\\ u^i-1, & i\ge 2,\text{even}\\ u^i-u, & i\ge 3,\text{odd}\end{cases},\quad -1\le u,v\le 1 \end{aligned} \tag{12}$$

(see Fig. 3 in [35] for visualization of these functions). Parameters N_u and N_v in (8) are the adopted degrees of the spatial polynomial approximation of the Hertz vector. The unitary vectors $\mathbf{a}_u$ and $\mathbf{a}_v$ in (12) are obtained as $\mathbf{a}_u(u,v)=\partial\mathbf{r}(u,v)/\partial u$ and $\mathbf{a}_v(u,v)=\partial\mathbf{r}(u,v)/\partial v$, with $\mathbf{r}$ given in (5), and $\mathfrak{I}$ is the Jacobian of the covariant transformation, $\mathfrak{I}(u,v)=|\mathbf{a}_u(u,v)\times\mathbf{a}_v(u,v)|$. Furthermore, we consider the functions in the following simplified form:

$$\mathbf{f}_{uij}(u,v)=\frac{\Gamma_{ij}(u,v)}{\mathfrak{I}(u,v)}\frac{\partial\mathbf{r}(u,v)}{\partial u},\ \mathbf{f}_{vij}(u,v)=\frac{\Gamma_{ij}(u,v)}{\mathfrak{I}(u,v)}\frac{\partial\mathbf{r}(u,v)}{\partial v}, \tag{13}$$

where Γ are the simple 2-D power functions,

$$\Gamma_{ij}(u,v)=u^iv^j\,. \tag{14}$$

Note that the lowest order of approximation ($N_u = N_v = 1$) yields the rooftop functions on generalized quadrilateral patches (which, for such basis functions, then must be very small).

Substituting (2)–(4) combined with (7)–(9) into (1) and applying the analytical expressions for the second derivative of the time dependent part of the Hertz vector h_{ij} (h_{ij} representing either h_{uij} or h_{vij}),

$$\frac{\mathrm{d}^2h_{ij}(t)}{\mathrm{d}t^2}=\sum_{q=0}^{M}\frac{s^2}{4}h_{ij,q}\left(\Psi_q(st)+2\Psi_{q+1}(st)+\Psi_{q+2}(st)\right), \tag{15}$$

with the first time-derivative being due to the magnetic vector potential term in (2) and the second due to the substitution of the surface current distribution in terms of the Hertz vector (7), the TDEFIE formulation can be finally expanded using unknown coefficients $h_{ij,q}$ and higher order temporal and spatial basis functions Ψ and $\mathbf{f}$, respectively, as follows:

$$\begin{aligned} &\Bigg[\frac{\mu s^2}{4\pi}\sum_{i=0}^{N_u}\sum_{j=0}^{N_v-1}\sum_{q=0}^{M}\left(h_{uij,q}+2h_{uij,q-1}+h_{uij,q-2}\right)\int_S\frac{1}{4R}\Psi_q(s\tau)\mathbf{f}_{uij}(\mathbf{r}')\mathrm{d}S\\ &-\frac{\nabla}{4\pi\varepsilon}\sum_{i=0}^{N_u}\sum_{j=0}^{N_v-1}\sum_{q=0}^{M}\left(h_{uij,q}-2h_{uij,q-1}+h_{uij,q-2}\right)\int_S\frac{1}{4R}\Psi_q(s\tau)\nabla'_s\cdot\mathbf{f}_{uij}(\mathbf{r}')\mathrm{d}S\\ &+\frac{\mu s^2}{4\pi}\sum_{i=0}^{N_u-1}\sum_{j=0}^{N_v}\sum_{q=0}^{M}\left(h_{vij,q}+2h_{vij,q-1}+h_{vij,q-2}\right)\int_S\frac{1}{4R}\Psi_q(s\tau)\mathbf{f}_{vij}(\mathbf{r}')\mathrm{d}S\\ &-\frac{\nabla}{4\pi\varepsilon}\sum_{i=0}^{N_u-1}\sum_{j=0}^{N_v}\sum_{q=0}^{M}\left(h_{vij,q}-2h_{vij,q-1}+h_{vij,q-2}\right)\int_S\frac{1}{4R}\Psi_q(s\tau)\nabla'_s\cdot\mathbf{f}_{vij}(\mathbf{r}')\mathrm{d}S\Bigg]_{\text{tang}}=(\mathbf{E}_{\mathrm{i}}(\mathbf{r},t))_{\text{tang}}. \end{aligned} \tag{16}$$

The closed form of the second derivative of the time dependent part of the Hertz vector (15) is derived satisfying the properties of Laguerre polynomials, i.e., causality and orthogonality [24], [36]. The error due to a finite difference approximation of this derivative, used in traditional MOT methods, is eliminated utilizing the analytical expression. In addition, there is no need for temporal interpolation of the solution. Once unknown coefficients are obtained, the current/field distribution over the SIE element can be

This article has been accepted for publication in a future issue of this journal, but has not been fully edited. Content may change prior to final publication. Citation information: DOI 10.1109/TAP.2015.2418343, IEEE Transactions on Antennas and Propagation

computed at any instant in time. Note that in (16), when compared to (9) and (15), the terms inside the temporal summation are regrouped with respect to unknown coefficients $h_{ij,q}$ instead of associated Laguerre functions Ψ_q.

D. Full Time-Space MoM Galerkin Testing

The TDEFIE (16) is tested by means of the full temporal and spatial Galerkin method [28], [29], [6] i.e., using the same functions used for current (Hertz-vector) expansion. The generalized Galerkin impedances corresponding, respectively, to the magnetic vector potential and electric scalar potential terms in the expression for the scattered field **E** in (2) in the model can be derived, using (3) and (4), in the following form:

$$Z^{A}_{mn,pq} = \frac{\mu}{4\pi}\int_{S_m}\int_{S_n}\int_{sR/c}^{\infty}\frac{1}{R}\mathbf{f}_m(u_m,v_m)\cdot\mathbf{f}_n(u_n,v_n)\Psi_p(st)\Psi_q(s\tau)\,\mathrm{d}(st)\,\mathrm{d}S_n\,\mathrm{d}S_m, \quad (17)$$

$$Z^{\Phi}_{mn,pq} = \frac{1}{4\pi\varepsilon}\int_{S_m}\int_{S_n}\int_{sR/c}^{\infty}\frac{1}{R}(\nabla\cdot\mathbf{f}_m(u_m,v_m))(\nabla\cdot\mathbf{f}_n(u_n,v_n))\Psi_p(st)\Psi_q(s\tau)\,\mathrm{d}(st)\,\mathrm{d}S_n\,\mathrm{d}S_m \quad (18)$$

where Ψ_p and Ψ_q are, respectively, the temporal testing and basis functions, p and q are indices/orders of the temporal testing and basis support, and $\mathbf{f}_m$ and $\mathbf{f}_n$ are the spatial testing and basis functions on the mth and nth generalized quadrilateral elements (S_m and S_n). The impedance in (18) is obtained applying the surface divergence theorem and the property of higher order divergence conforming functions that the normal component of the testing function $\mathbf{f}_m$ is either zero at the element edges or the two contributions of the elements sharing an edge exactly cancel out in the final expressions for generalized impedances. The source-to-field distance R in (17) and (18) is computed as $R = |\mathbf{r}_m(u_m,v_m) - \mathbf{r}_n(u_n,v_n)|$, with $\mathbf{r}$ being defined in (5).

Due to causality and orthogonality of Laguerre polynomials [24], temporal integrals in (17) and (18) can be handled analytically first, resulting in the two types of Green's functions for 2-D spatial integrals, as follows

$$I_{pq}(sR/c) = \int_{sR/c}^{\infty}\Psi_p(st)\Psi_q(st-sR/c)\,\mathrm{d}(st) = \begin{cases} \mathrm{e}^{-sR/(2c)}, & q=p \\ \mathrm{e}^{-sR/(2c)}(L_{p-q}(sR/c)-L_{p-q-1}(sR/c)), & q<p \\ 0, & q>p. \end{cases} \quad (19)$$

Taking into account the parametric representation of the quadrilateral surface element, in (5), and simplified representation of the spatial basis functions in (13) and (14), generalized impedance terms in (17) and (18) corresponding to the testing functions defined by indices i_m and j_m on the mth quadrilateral and the basis function defined by indices i_n and j_n on the nth quadrilateral become

$$Z^{A,i}_{mn,pq}(i_m,j_m,i_n,j_n) = \sum_{k_m=1}^{K_u^{(m)}}\sum_{l_m=0}^{K_v^{(m)}}\sum_{k_n=1}^{K_u^{(n)}}\sum_{l_n=0}^{K_v^{(n)}} k_m k_n \mathbf{r}_{kl}^{(m)}\cdot\mathbf{r}_{kl}^{(n)} \cdot\xi_i(i_m+k_m-1, j_m+l_m, i_n+k_n-1, j_n+l_n), \quad (20)$$

$$Z^{\Phi,i}_{mn,pq}(i_m,j_m,i_n,j_n) = i_m i_n \xi_i(i_m-1,j_m,i_n-1,j_n), \quad i_m=0,1,\ldots,N_u^{(m)},\quad j_m=0,1,\ldots,N_v^{(m)}, \quad i_n=0,1,\ldots,N_u^{(n)},\quad j_n=0,1,\ldots,N_v^{(n)},\quad i=1,2. \quad (21)$$

In these equations, $N_u^{(m)}$ and $N_v^{(m)}$ are the Hertz-vector approximation orders of the mth quadrilateral along the u- and v-coordinate, respectively, $N_u^{(n)}$ and $N_v^{(n)}$ are the corresponding orders for the nth quadrilateral, and the integration limits in both quadrilaterals are $u_1 = v_1 = -1$ and $u_2 = v_2 = 1$. In addition, $K_u^{(m)}$ and $K_v^{(m)}$ are the geometrical orders along the u- and v-coordinate, respectively, $\mathbf{r}_{kl}^{(m)}$ are the geometrical vector coefficients in the polynomial expansion of the mth quadrilateral, $K_u^{(n)}$, $K_v^{(n)}$, and $\mathbf{r}_{kl}^{(n)}$ are the corresponding geometrical parameters for the nth quadrilateral in the model, and ξ_i is the basic Galerkin potential integral given by

$$\xi_i(i_m,j_m,i_n,j_n) = \int_{u_{1m}}^{u_{2m}}\int_{v_{1m}}^{v_{2m}}\int_{u_{1n}}^{u_{2n}}\int_{v_{1n}}^{v_{2n}} u_m^{i_m} v_m^{j_m} u_n^{i_n} v_n^{j_n} g_i(R)\,\mathrm{d}u_n\,\mathrm{d}v_n\,\mathrm{d}u_m\,\mathrm{d}v_m, \quad i=1,2 \quad (22)$$

The ξ_1-type integral [for i = 1 in (22)], involving the first Green's function based on (19), $g_1(R) = I_{pq}(sR/c)/\mathrm{R} = \mathrm{e}^{-sR/(2c)}/R$, when $q = p$, has a $1/R$-type singularity, which is taken care of as in our frequency-domain (FD) MoM-SIE methods [28], [29]. The ξ_2-type integral [for i = 2 in (22)], with the second Green's function $g_2(R) = I_{pq}(sR/c)/\mathrm{R} = \mathrm{e}^{-sR/(2c)}(L_{p-q}(sR/c) - L_{p-q-1}(sR/c))/R$ when $q < p$, is not singular for R approaching zero, since $\lim_{R\to 0} g_2(R) = -s/c$; this can be proved by applying L'Hospital's rule and properties of the Laguerre polynomials.

The generalized Galerkin voltages, namely, the column-matrix elements due to the incident field on the right-hand side of the equation (16), are evaluated, after the temporal and spatial Galerkin testing, as

$$V^{i}_{m,p} = \int_{S_m}\mathbf{f}_m\cdot\int_{t=0}^{\infty}\Psi_p(st)\mathbf{E}_{\mathrm{i}}(\mathbf{r},t)\,\mathrm{d}(st)\,\mathrm{d}S_m. \quad (23)$$

In order to compute the temporal integral in (23) numerically, the upper limit is truncated to a finite duration of the time-domain signature T_{f} multiplied by the scaling factor s, ensuring that all further transient variations in the spatial domain of interest can be neglected.

Finally, the generalized Galerkin impedances corresponding to the complete set of spatial basis functions in (12) can be obtained as a linear combination of those in (20) and (21), corresponding to the simplified functions in (13) and (14), and

This article has been accepted for publication in a future issue of this journal, but has not been fully edited. Content may change prior to final publication. Citation information: DOI 10.1109/TAP.2015.2418343, IEEE Transactions on Antennas and Propagation

similarly for the generalized voltages, which greatly expedites the matrix fill process when compared to the direct computation of final impedances and voltages [29]. Moreover, the Galerkin impedances and voltages for any higher order set of basis functions of divergence-conforming polynomial type can also be constructed as a linear combination of the impedances for the simple 2-D power functions in (13) and (14).

E. MOD solution of MoM-TD EFIE

After Galerkin testing of (16) in space-time, with all generalized impedance and voltage matrices in (20)–(23) being already precalculated, the global system of linear algebraic equations can be obtained in the following form:

$$\begin{aligned}
&[Z_{mn}]\{h_{n,p}\} = \{V^{\mathrm{i}}_{m,p}\} - [Z^{A,1}_{mn}](2\{h_{n,p-1}\} + \{h_{n,p-2}\}) \\
&-[Z^{\Phi,1}_{mn}](\{h_{n,p-2}\} - 2\{h_{n,p-1}\}) \\
&-\sum_{q=0}^{p-1}[Z^{A,2}_{mn,M-p+q}](\{h_{n,q}\} + 2\{h_{n,q-1}\} + \{h_{n,q-2}\}) \\
&-\sum_{q=0}^{p-1}[Z^{\Phi,2}_{mn,M-p+q}](\{h_{n,q}\} - 2\{h_{n,q-1}\} + \{h_{n,q-2}\}), \\
&p = 0,1,\ldots,M, \quad q = 0,1,\ldots,p-1, \\
&m = 1,2,\ldots,N_{\mathrm{MoM}}, \quad n = 1,2,\ldots,N_{\mathrm{MoM}},
\end{aligned} \tag{24}$$

where $[Z_{mn}]=[Z^{A,1}_{mn}]+[Z^{\Phi,1}_{mn}]$ is the system matrix, which takes into account contributions of the generalized impedance matrices, from (20) and (21) (for $[Z^{A,1}_{mn}]$ and $[Z^{\Phi,1}_{mn}]$, respectively), for the ξ_1-type integral from (22) combined with (19) for the cases when $q = p$. As can be seen, the system matrix does not depend on the orders of temporal testing and basis functions, p and q, respectively; therefore, it is computed and inverted only once. Generalized impedances (20) and (21) corresponding to the ξ_2-type integral, with (22) combined with (19) for the cases when $q < p$, are precalculated for each combination of the temporal testing and basis function indices, p and q, and stored in 3-D matrices constituted by M-element arrays of 2-D matrices $[Z^{A,2}_{mn,k}]$ and $[Z^{\Phi,2}_{mn,k}]$, $k = M - p + q$, of size $m \times n = N_{\mathrm{MoM}} \times N_{\mathrm{MoM}}$, with M being the order of temporal basis functions and N_{MoM} the total number of MoM spatial unknowns. The minimal order M is defined by the time duration, T_{f}, and the frequency bandwidth, B, of the excitation so that $M \geq 2BT_{\mathrm{f}} + 1$ [19], [21]. Finally, the system (24) is solved recursively in the marching-on-in-degree (MOD) fashion for unknown coefficients of the Hertz vector $\{h_{n,p}\}$, $n = 1, 2, \ldots, N_{\mathrm{MoM}}$, $p = 0, 1, 2, \ldots, M$. Note that, comparing (24) with (16), the temporal summation on the right-hand side of the system equation (which includes already known coefficients) is done up to $p - 1$ instead of M because of the property (19), $I_{pq}(sR/c) = 0$ when $q > p$. Note also that initial coefficients for $p = 0$, $\{h_{n,0}\}$, are obtained as the solution of the matrix equation $[Z_{mn}]\{h_{n,0}\} = \{V^{\mathrm{i}}_{m,0}\}$. In this case, the only contribution from the right-hand side of the system (24) is due to the excitation vector $\{V^{\mathrm{i}}_{m,0}\}$, while all other terms are equal to zero because of the causality property of Laguerre polynomials. The system of equations (24) for the pth order is solved by Gaussian elimination for unknown coefficients $\{h_{n,p}\}$. By postprocessing of the obtained coefficients, the current $\mathbf{J}_{\mathrm{s}}$ over any generalized quadrilateral patch in the model is computed using (7), where the first derivative of $h_n(t)$ is calculated analytically as

$$\frac{\mathrm{d}h_n(t)}{\mathrm{d}t} = \sum_{q=0}^{M}\frac{s}{2}h_{n,q}\left(\Psi_q(st) - \Psi_{q+2}(st)\right). \tag{25}$$

Computation of electric and magnetic fields due to $\mathbf{J}_{\mathrm{s}}$, as well as of any other quantity of interest for the analysis, is then straightforward.

III. Numerical Results and Discussion

In this section, five PEC scattering structures in free space are analyzed to validate and evaluate the proposed spatially large-domain and temporally entire-domain MoM-MOD TD EFIE method. In all the examples, we solve for the induced transient surface current densities, as the most rigorous representative of the solution accuracy, critical for all near field parameters and quantities. Generally, the accuracy of far field computations is much better than that for the current distribution. All the structures are illuminated by an incident Gaussian pulse as shown in Fig. 3 and given by

$$\mathbf{E}_{\mathrm{i}}(\mathbf{r},t) = \mathbf{E}_0\frac{4}{T_{\mathrm{w}}\sqrt{\pi}}\mathrm{e}^{-\gamma^2}, \quad \gamma = \frac{4}{T_{\mathrm{w}}}(c_0t - c_0t_0 - \mathbf{r}\cdot\hat{\mathbf{k}}), \tag{26}$$

where the vector amplitude $\mathbf{E}_0$ takes into account the polarization of the wave, $\hat{\mathbf{k}}$ is the unit vector in the propagation direction of the incident wave, $\mathbf{r}$ is the position vector of the observation point with respect to the global

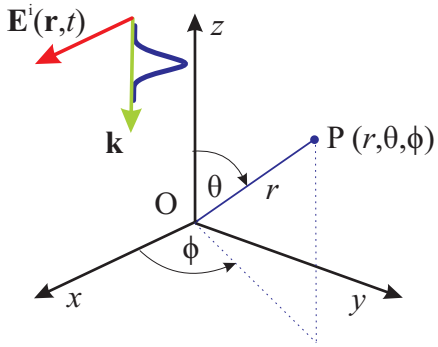

Fig. 3. Incident Gaussian pulse defined in (26) (shown for $\mathbf{E}_0 = E_0\hat{\mathbf{x}}$ and $\hat{\mathbf{k}} = -\hat{\mathbf{z}}$) and associated spherical coordinate system defining elevation and azimuthal angles, θ and ϕ, respectively – as excitation of conducting scatterers analyzed by the MoM-MOD method.

This article has been accepted for publication in a future issue of this journal, but has not been fully edited. Content may change prior to final publication. Citation information: DOI 10.1109/TAP.2015.2418343, IEEE Transactions on Antennas and Propagation

coordinate origin, c_0 is the speed of light, t_0 represents a time delay of the Gaussian peak from the time origin, and T_w is the width of the Gaussian pulse. Time units in the examples are expressed in terms of light meters (lm), where $t\,[\text{lm}]=c_0 t$.

As the first example, we perform the convergence analysis of the new MoM-MOD method for a metallic square plate with edge length $a = 2$ m. Excitation is by a Gaussian pulse (Fig. 3) normally impinging on a plate with $E_0 = 1$ V/m, $T_w = 4$ lm, and $t_0 = 6$ lm. The wave is linearly polarized with its electric field vector being parallel to one pair of plate edges. We consider in all examples that the pulse has significant spectral components up to f_{max} where the spectral amplitude decays to 0.1% of the maximal value. In this example it is approximately $f_{max} = 250$ MHz. We consider two models of the first geometrical order ($K_u = K_v = K = 1$) for the plate scatterer: (A) plate subdivided into 3 × 3 equal square SIE elements, of electrical size $e_A = a/3 = 0.556\lambda$ (λ being the free-space wavelength) at f_{max}, and (B) entire-domain model of the plate with a single SIE element, of electrical size $e_B = a = 1.667\lambda$ at f_{max} [note that even e_A in model (A) is approximately six times larger than the size of elements used in low-order small-domain MoM techniques, $e_{\text{small-domain}} \approx 0.1\lambda$]. First, we investigate the optimal order of temporal basis functions, varying M in model (A) from 10 to 80, for a fixed order of spatial basis functions $N_u = N_v = N = 4$ (an overly safe choice based on our study of higer order parameters for the MoM-FD SIE method in [37]), which results in a total of $N_{MoM} = 264$ spatial unknowns, and a fixed scaling factor $s = 10^9$. Fig. 4(a) shows that $M = 30$ is sufficient for accurate results. Next, shown in Fig. 4(b) is the p-refinement of model (B), with N ranging from 2 to 5, for the fixed order of temporal current approximation $M = 30$ and scaling factor $s = 10^9$, so chosen to provide accurate transient solution. Note that parameters M and s are the same as for model (A); as expected, they are not influenced by the size of the element, only parameter N is. The higher order results are compared with a low-order MoM-MOT solution [13], which includes 112 flat triangular patches and 153 spatial unknowns (the surface current density is approximated using RWG spatial basis functions and triangular temporal basis functions). We observe from the figure that the higher order results converge monotonically and quickly with the p-refinement and that the solution corresponding to $N = 5$, resulting in $N_{MoM} = 40$ unknowns only, agrees very well with the reference solution. With the entire-domain model (B), N_{MoM} is reduced by a factor of 6.6 with respect to model (A) with $N = 4$, and by a factor of 3.8 when compared to the reference solution [13].

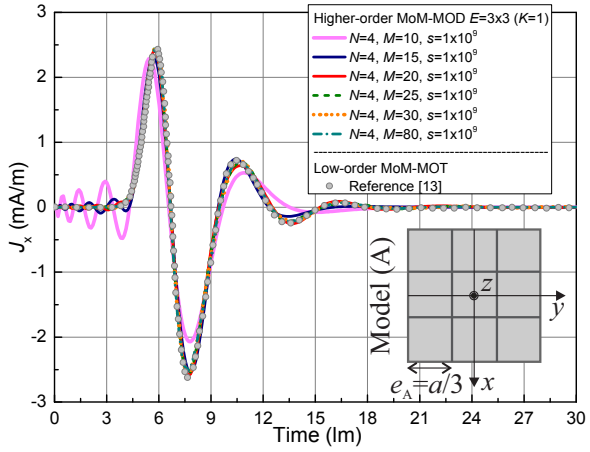

(a)

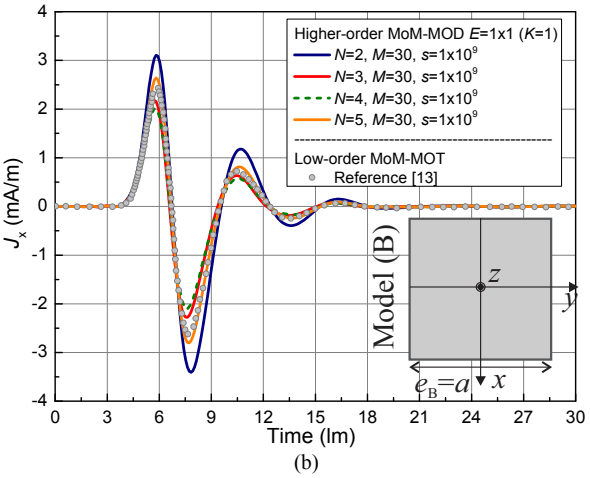

(b)

Fig. 4. Convergence analysis of the presented MoM-MOD method for a metallic square plate scatterer in terms of the orders of temporal and spatial basis functions, M and $N_u = N_v = N$, in computing transient responses of the x-directed surface current density at the center of the plate: (a) increasing M for a fixed N in model (A) (plate subdivided into 3 × 3 SIE elements) and (b) p-refinement of model (B) (entire-domain model, with a single SIE element) for a fixed M. The higher order results are compared with the low-order MoM-MOT solution [13].

As the second example of structures with flat surfaces and sharp edges, we consider the transient current response over sides of a PEC cube of edge length $a = 1$ m. For the incident wave in (26), $\mathbf{E}_0 = E_0\hat{\mathbf{x}}$, ($E_0 = 1$ V/m) and $\hat{\mathbf{k}} = -\hat{\mathbf{z}}$, which corresponds to the azimuthal angle $\phi = 0^o$ and elevation angle $\theta = 0^o$, as depicted in Fig. 3, and the Gaussian pulse is defined for two different cases of the analysis. In case (i), we adopt $T_w = 8$ lm and $t_0 = 12$ lm, so that the pulse frequency spectrum has a practical upper bound of $f_{max1} = 125$ MHz, and thus its band does not contain internal resonances of the cube, the lowest of which occurs at $f_{res1} = 212.13$ MHz. For case (ii), $T_w = 2$ lm and $t_0 = 3$ lm, resulting in the upper frequency bound of $f_{max2} = 500$ MHz for the covered frequency band, which includes the first six resonances of the cube ($f_{res2} = 259.81$ MHz, $f_{res3} = 335.41$ MHz, $f_{res4} = 367.42$ MHz, $f_{res5} = 424.26$ MHz, $f_{res6} = 450.00$ MHz). For the temporal approximation in the method, we adopt $M = 130$ and $s = 10^8$ in case (i) and $s = 3\times10^8$ in case (ii). In addition, we consider two different spatial models of the cube: (A) the cube subdivided uniformly with three subdivisions per edge, which results in 54 flat ($K_u = K_v = K = 1$) quadrilateral patches (squares) (note that $e_A = a/3 \approx 0.13\lambda$ at f_{max1}), with $N_u = N_v = N = 2$ and $N_{MoM} = 432$ and (B) the cube modeled using only six flat surface elements representing the six cube faces ($e_B = a = 0.42\lambda$ at f_{max1} and $e_B = a = 1.667\lambda$ at f_{max2}), with $N = 5$ and $N_{MoM} = 300$. Figs. 5(a) and (b)–(c) show, respectively, the transient current responses in the nonresonant

This article has been accepted for publication in a future issue of this journal, but has not been fully edited. Content may change prior to final publication. Citation information: DOI 10.1109/TAP.2015.2418343, IEEE Transactions on Antennas and Propagation

band [excitation case (i)] obtained simulating both models (A) and (B) and the resonant band [excitation case (ii)] using model (B) only. The higher order MoM-MOD results are compared with low-order implicit MoM-MOT TD CFIE solutions (using 832 triangular patches and 1,248 spatial unknowns) reported in [38], and an excellent agreement of the two sets of results is observed.

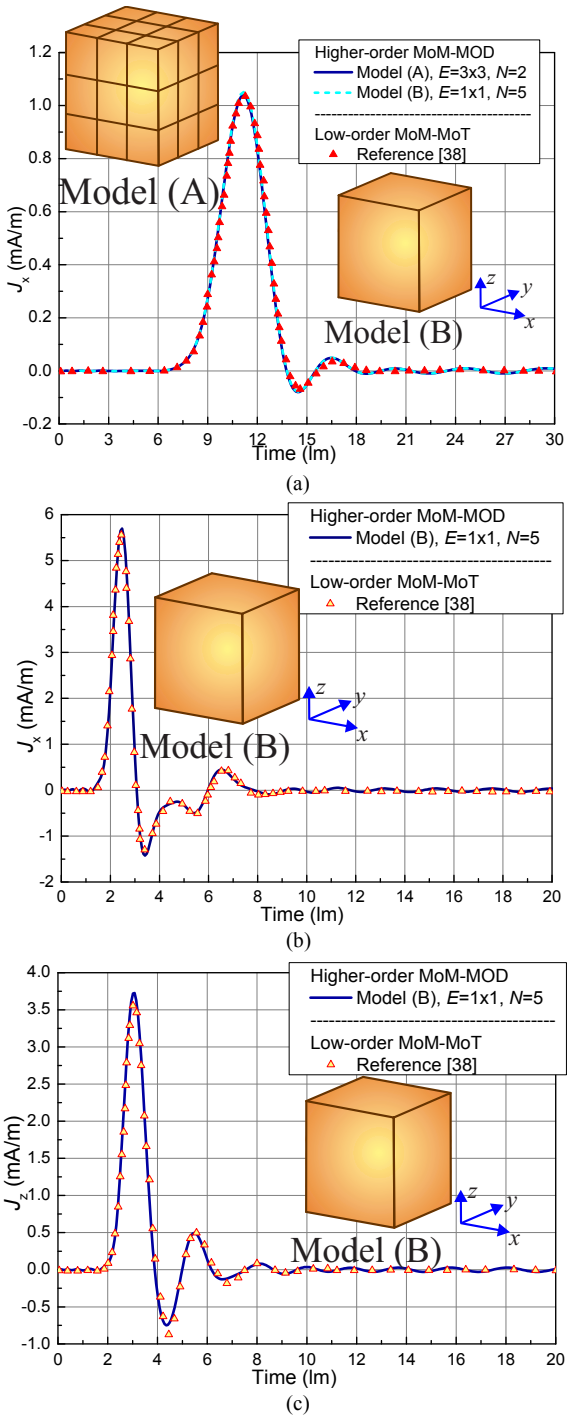

Fig. 5. Comparison of results obtained by the presented MoM-MOD TD EFIE method and low-order implicit MoM-MOT TD CFIE solutions [38] for the transient current response of a PEC cubical scatterer: (a) x-directed surface current density at the center of the top face of the cube in the nonresonant band [excitation case (i)] for two different models (A) and (B) shown in the inset; and (b) x-directed J_S at the center of the top face and (c) z-directed J_S at the center of the side face of the cube in the resonant band [excitation case (ii)] using model (B) only.

As the first example of structures with pronounced curvature, we next analyze a metallic spherical scatterer, of radius $a = 0.5$ m, illuminated as in Fig. 3 with $\mathbf{E}_0 = E_0\hat{\mathbf{x}}$, ($E_0 = 1$ V/m), $\hat{\mathbf{k}} = -\hat{\mathbf{z}}$, finite duration of the signal $T_f = 40$ lm, and cases (i) and (ii) from the previous example (note that the first three internal resonances of the sphere are $f_{res1} = 262.02$ MHz, $f_{res2} = 369.77$ MHz, and $f_{res3} = 429.06$ MHz). Spatial modeling of the sphere is performed using only six equal generalized quadrilateral SIE patches with geometrical orders (A) $K_u = K_v = K = 2$ and (B) $K = 4$, respectively ($e_A = e_B \approx 0.36\lambda$ at f_{max1} and $e_A = e_B \approx 1.34\lambda$ at f_{max2}). Figs. 6(a) and (b) show the convergence of the presented MoM-MOD method with respect to polynomial orders of spatial and temporal approximations, respectively, of the z-component of $\mathbf{J}_S$ at the center of one of the six patches (this point belongs to the central equator of the sphere) in model (A) in excitation case (i). Based on these results, the optimal polynomial orders of spatial and temporal basis functions of the Hertz vector (current), in (8) and (9), are found to be $N_u = N_v = N = 2$, which yields $N_{MoM} = 48$, and $M = 130$ (with $s = 10^8$), respectively, for this example, and the agreement with results obtained by a low-order MoM-TD EFIE technique (528 flat triangular patches and 792 spatial unknowns) in conjunction with a conventional MOD [20] is observed to be excellent. The convergence of the higher order results in terms of the geometrical order of modeling for excitation case (ii), where $N = 4$ and only 192 unknowns suffice, is presented in Fig. 6(c). Both models (A) and (B) provide an excellent accuracy of results when compared to the reference solution [20], but the results obtained with $K = 4$ can be observed to be in a better agreement with the reference solution at the current peak than those with $K = 2$. Note also that the more accurate curved geometrical model with only six higher order SIE elements reduces the number of spatial unknowns by a factor of 16.5 in case (i), and by a factor of 4.1 in case (ii), when compared to the reference model [20].

To examine the convergence of the presented MoM-MOD with spatial refinement (h-refinement), in Fig. 7 we plot the relative error of the current, with respect to the analytical solution obtained by Mie series, for the sphere from Fig. 6(c), in the frequency domain. The frequency domain current is obtained from the MoM-MOD solution using DFT and the relative error with respect to Mie series is averaged in the frequency range from 25 MHz to 300 MHz as

$$\text{Error}[\%] = \frac{1}{N_f}\sum_{i=1}^{N_f}\left|\frac{\mathrm{J}_i^{\mathrm{SIE}}(\theta,\phi)}{\mathrm{J}_i^{\mathrm{Mie}}(\theta,\phi)} - 1\right| \cdot 100\,, \qquad (27)$$

where $N_f = 12$ is the number of frequency samples, for fixed $\theta = 90^o$ and $\phi = 180^o$ defining the point on the spherical surface in which the currents are computed and compared. The figure shows a family of curves with three representative polynomial current approximations $N = 2$, $N = 3$, and $N = 5$, kept constant for all elements in respective meshes. The points on the $N = 2$ curve correspond, from left to right, to each of the six faces of the sphere from Fig. 6(c) being uniformly

This article has been accepted for publication in a future issue of this journal, but has not been fully edited. Content may change prior to final publication. Citation information: DOI 10.1109/TAP.2015.2418343, IEEE Transactions on Antennas and Propagation

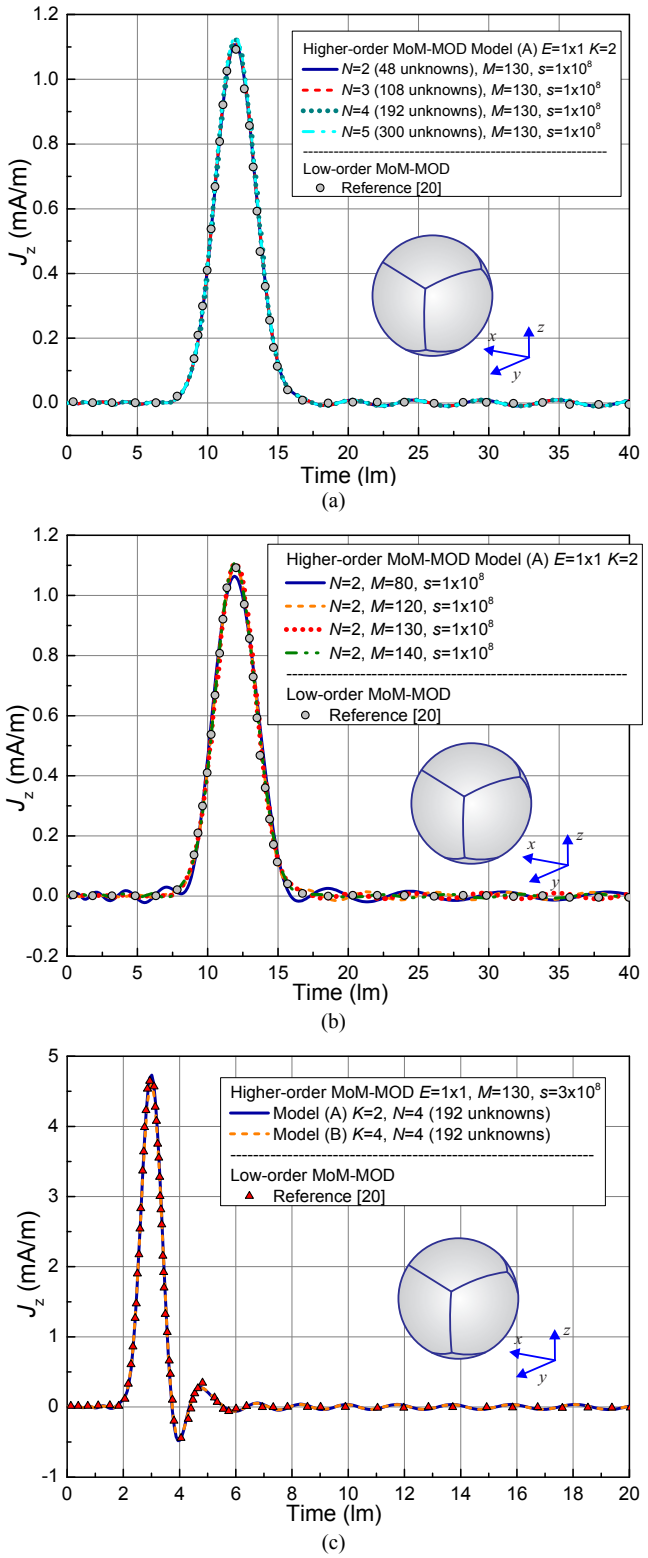

Fig. 6. Convergence of results for a metallic spherical scatterer obtained by the presented MoM-MOD method with respect to polynomial orders of (a) spatial and (b) temporal approximations of the z-component of $\mathbf{J}_S$ at the center of one of the six patches in model (A) ($K_u = K_v = K = 2$) shown in the figure inset in the nonresonant band [excitation case (i)], and (c) convergence of the method in terms of the geometrical order K of modeling in the resonant band [excitation case (ii)]. The higher order solutions are compared with results using the low-order MoM-MOD method [20].

refined into 2×2, 4×4, and 6×6 elements, respectively. Similarly, the points on the $N=3$ curve correspond to a refinement of each of the faces into 1×1, 2×2, and 4×4 elements, and finally the points on the $N=5$ curve correspond to a refinement of each of the faces into 1×1 and 2×2 elements. All meshes are shown in the figure inset.

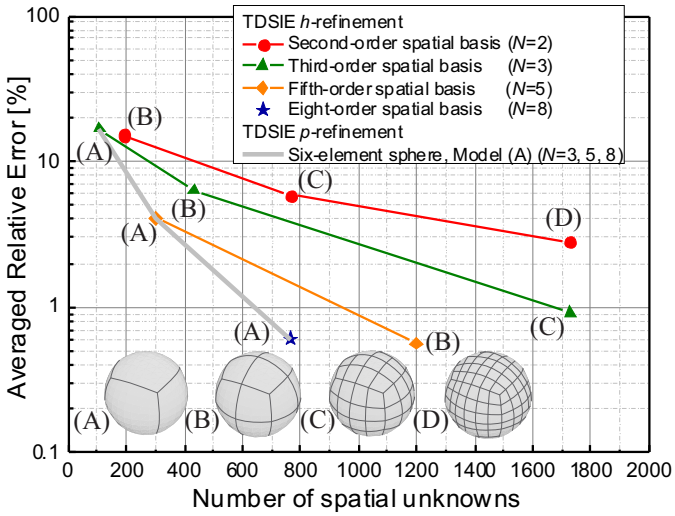

Fig. 7. Relative error of the TDSIE MoM-MOD computed frequency-domain current averaged in the frequency range from 25 MHz to 300 MHz vs. the number of (spatial) MoM unknowns. A family of three curves obtained using models with three constant polynomial expansion orders N across all the elements shows convergence of the solution with an h-refinement of the mesh, while the fourth curve shows p-refinement of the solution for geometrical model (A).

We observe from Fig. 7 that the method yields monotonic convergence with h-refinement and that higher order polynomial current approximation yields better convergence than the lower order expansion. Note also that in this example our lowest achievable error is around 0.55%, which is consistent with the lowest errors achieved by the CFIE based MOT for the PEC sphere example reported in [6]. At the same time, we remark that the error of 0.56%, i.e., close to the minimum error limit, is achieved very quickly with $N=5$ in our example, hence only two points are shown on this curve. We finally note that our solution with the 0.55% error in computed current yields 0.05% relative error in the computation of the radar cross section (RCS), which is consistent with the lowest reported errors in [5]. In addition, we show in Fig. 7 p-refinement of the solution for three different spatial current approximation orders N = 3, 5, and 8 on the same geometrical model, model (A), with only six large SIE elements of the fourth geometrical order, K = 4 (element size is $e \approx 1.34\lambda$ at f_{max2}). Note that model (A) with N = 8 reduces the number of spatial unknowns 1.56 times when compared to model (B) with N = 5 while maintaining almost the same accuracy, the error being 0.61%. Also, when compared to model (C) with N = 2 for the same number of spatial unknowns (N_{MoM} = 768), the error is reduced 10 times.

Investigating further the convergence of the MoM-MOD with increasing the maximal order of the time domain basis M, shown in Fig. 8 is the averaged relative error of the frequency-domain current (computed with respect to the analytical Mie series solution in the same way as for the example in Fig. 7, using (27)). The family of curves in Fig. 8 is chosen as

This article has been accepted for publication in a future issue of this journal, but has not been fully edited. Content may change prior to final publication. Citation information: DOI 10.1109/TAP.2015.2418343, IEEE Transactions on Antennas and Propagation

follows. Starting from the first curve on the top (curve I), we have a mesh where each of the 6 sphere faces is divided into 3×3 elements, model (E), with the polynomial current approximation order $N = 2$, which yields 54 elements and $N_{\text{MoM}} = 432$ unknowns. This mesh is then *h*-refined, so that the 6 sphere faces are divided into 6×6 elements, model (D) in Fig. 7, and the polynomial current approximation order is kept the same ($N = 2$), which results in 216 elements and $N_{\text{MoM}} =$ 1,728 unknowns, and the error of the model in this arrangement is given via the second curve from the top (curve II). The third curve from the top (curve III) is obtained utilizing a mesh where each of the 6 sphere faces is divided into 2×2 elements, model (B) in Fig. 7, with the polynomial current approximation order $N = 4$, which yields 24 elements and $N_{\text{MoM}} = 768$ unknowns. Similarly as before, this mesh is *h*-refined so that the 6 sphere faces are divided into 3×3 elements, model (E) in Fig. 8, and the polynomial current approximation order is kept the same ($N = 4$), which gives 54 elements and $N_{\text{MoM}} =$ 1,728 unknowns, and the error of the model in this arrangement is shown as the bottom curve (curve IV).

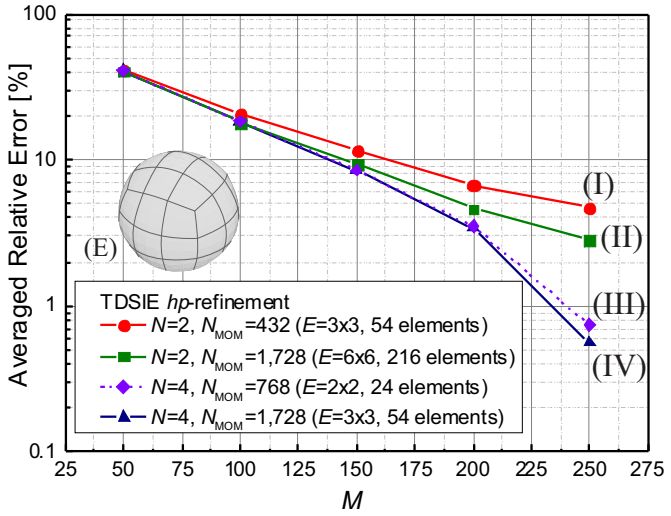

Fig. 8. Relative error of the TDSIE MoM-MOD computed frequency-domain current averaged in the frequency range from 25 MHz to 300 MHz vs. the order of the time-domain bases *M*. Two sets of curves, with polynomial expansion orders across all the elements in the mesh equal to $N = 2$ and $N = 4$, both shown for models with a coarse and an *h*-refined mesh, demonstrate the convergence of the solution with respect to *p*- and *h*-refinement, as well as with increase of the temporal bases order, *M*.

We conclude from Fig. 8 that increasing *M*, i.e, marching-on-in-degree, yields monotonic convergence in all cases. At the same time, we see that *h*-refinement (e.g., going from curve I to curve II) yields only slightly lower error (about 2%) while increasing the number of unknowns four times. Similarly, going from curve III to curve IV, the error decreases only slightly while more than doubling (2.25 times) the number of unknowns. (Note that the minimal error is practically reached for $M = 250$ in both curve III and curve IV.) On the other hand, going from curve I to curve III, by increasing *N* from 2 to 4, i.e., with a *p*-refinement of the solution, much faster convergence is achieved while the number of unknowns is increased only about 1.78 times.

The next example presents the higher order MoM-MOD transient analysis of a standard benchmarking structure – NASA almond [39] of the maximum length (from the tip to the tail of the almond) $l_{\max} = 1$ m, illuminated as in Fig. 3 with $\mathbf{E}_0 = 377$ V/m $\hat{\mathbf{x}}$, $\hat{\mathbf{k}} = -\hat{\mathbf{z}}$, $T_{\text{f}} = 30$ lm, $T_{\text{w}} = 4$ lm, $t_0 = 6$ lm, and $f_{\max} = 250$ MHz. The almond is modeled using only 56 quadrilateral surface elements ($e \leq 0.1\lambda$ at $f_{\max}$) of second geometrical order ($K_u = K_v = K = 2$), as portrayed in Fig. 9(a), and the other numerical parameters of the model are $N_u = N_v = 2$, $N_{\text{MoM}} = 448$, $M = 130$, and $s = 3 \times 10^8$. Shown in Fig. 9(b) is the transient response of the current density at the center of the top surface of the almond. The results obtained by the presented MoM-MOD are compared with a low-order MoM-MOD solution (864 flat triangular elements, 1,296 spatial unknowns, and $M = 128$) [40], and we observe an excellent agreement of the two sets of MoM-MOD results.

As the last example, we analyze a more complex structure such as a military tank of dimensions 4 m × 9 m × 2.73 m, shown in Fig. 10(a). The structure is illuminated with a θ-polarized Gaussian pulse of amplitude $E_0 = 1$ V/m impinging from the direction defined by $\theta = 90^{\text{o}}$ and $\phi = 0^{\text{o}}$ (Fig. 3), with $T_{\text{w}} = 70$ lm, $t_0 = 90$ lm, and $f_{\max} = 15$ MHz. The tank is modeled using only 147 surface elements with $K_u = K_v = K = 1$ [as indicated in Fig. 10(a)] and $e_{\max} \approx 0.315\lambda$ at $f_{\max}$. The transient response of $\mathbf{J}_{\text{S}}$ at the center of a flat patch on the tank

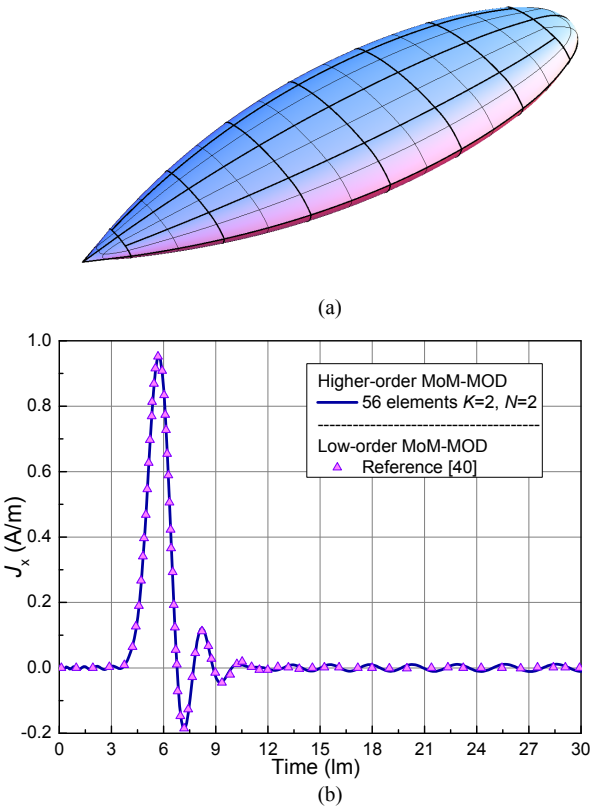

Fig. 9. MoM-MOD scattering analysis of the NASA metallic almond: (a) geometrical model with 56 curved quadrilateral SIE patches and (b) comparison of results for the transient response of the *x*-directed surface current density at the center of the top face of the almond obtained by the presented MoM-MOD and the low-order MoM-MOD solution [40].

This article has been accepted for publication in a future issue of this journal, but has not been fully edited. Content may change prior to final publication. Citation information: DOI 10.1109/TAP.2015.2418343, IEEE Transactions on Antennas and Propagation

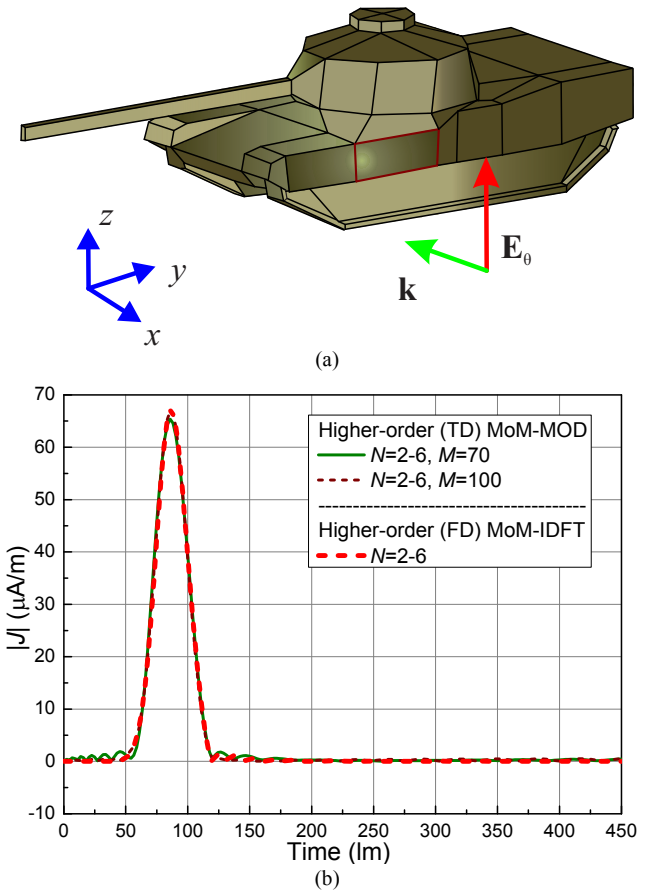

Fig. 10. (a) WIPL-D mesh of a military tank consisting of 147 quadrilateral patches with $K_u = K_v = K = 1$ [41] and (b) transient response of $\mathbf{J}_S$ at the center of a flat patch on the tank side marked by the red frame computed using the presented MoM-MOD TD SIE method and the higher order MoM-FD SIE method [29] in conjunction with the inverse discrete Fourier transform.

side marked by the red frame in Fig. 10(a) is computed using the presented MoM-MOD algorithm with N ranging from 2 to 6, $N_{\text{MoM}} = 1{,}389$, $s = 1\times10^8$, and $M = 70$ or 100. The solution is compared in Fig. 10(b) with frequency-domain results obtained using the higher order MoM-FD SIE method [29] in conjunction with the inverse discrete Fourier transform (IDFT) and computed from DC (extrapolated) to 50 MHz at 128 frequency samples; an excellent agreement of the TD and FD sets of results is observed. For exactly the same spatial model, the computational time for the MoM-FD SIE simulation is 125 min, while the MoM-TD SIE simulation with $M = 70$ takes less than 3 min (computer properties: Intel® Xeon® CPU E5645 @ 2.40 GHz). Note that a similar tank model is analyzed in [26] using low-order small-domain MoM-MOD EFIE and MoM-MOT methods. The model in [26] includes 2,737 triangular flat patches, the spatial distribution of $\mathbf{J}_S$ is expanded in terms of RWG basis functions resulting in 3,905 unknowns, the order of temporal basis functions is $M = 30$, and the excitation is in the form of a triangular pulse with the frequency bandwidth of 50 MHz. The reported simulation times for this model are 1,012 min and 938 min for the MoM-MOD and MoM-MOT methods, respectively. With an assumption that the simulations in [26] are performed on a standard PC with similar or closely comparable hardware (computer used is not specified in [26]), we may conclude that the present method comes out to be much more efficient than methods in [26].

IV. Conclusions

This paper has proposed and presented the first spatially and temporally higher order MoM-TD method with very high spatial and temporal expansion orders; the results demonstrate using current expansions of spatial orders from 2 to 8 in conjunction with using entire-domain Laguerre polynomial temporal basis functions, and geometrical-mapping orders from 1 to 4. In that regard, this work is different when compared to practically all the existing MOT and MOD MoM-TD tools, which use planar triangular patches and RWG functions. In that regard, it also is different when compared to higher order MoM-TD MOT techniques [30]–[32] and [5].

In addition, the proposed method is the first spatially higher order MoM-TD MOD method. In that regard, this work is different when compared to all the existing spatially higher order MoM-TD methods in literature, which all are MOT methods.

The paper has proposed and presented the first spatially large-domain MoM-TD method. In that regard, this work is different when compared to all the existing spatially higher order MoM-TD MOT methods in literature, which all can be considered as small-domain (subdomain) methods, with the EM structure being modeled by surface elements that are electrically very small. The paper has presented the first set of spatially large-domain MoM-TD modeling examples; the electrical sizes of flat and curved patches in models are up to about 1.7 wavelengths at the maximum frequency in the frequency spectrum of the pulse excitation.

It turns out that the MOD methodology is a particularly suitable choice if combined with higher order spatial elements, large-domain modeling, and p-refined solutions.

The paper has presented transient analysis using electrically large (and small) elements in combination with higher order spatial and temporal basis functions which significantly reduces the number of spatial unknowns when compared to low-order small-domain methods with no accuracy trade-off; this has been shown in all numerical examples in the paper. This unique property – computational efficiency improvement of this method – has not been shown in other transient methods, MOT and MOD.

Also, superior efficiency of the higher order MoM-TD MOD method as compared to the higher order MoM-FD method in conjunction with the IDFT – in transient analysis on exactly the same spatial model – has been demonstrated in Fig. 10 (the tank model). In this example, the TD code is about 42 times faster than the FD code. Although TD codes should, naturally, be more efficient in transient analysis than FD codes, this result is better than what was anticipated, especially since a quite high order of temporal bases ($M = 70$) is used.

Convergence analysis (based on the relative error of the current with respect to the analytical solution obtained by Mie series) in Figs. 7 and 8 has demonstrated the convergence of

This article has been accepted for publication in a future issue of this journal, but has not been fully edited. Content may change prior to final publication. Citation information: DOI 10.1109/TAP.2015.2418343, IEEE Transactions on Antennas and Propagation

the solution with respect to *h*- and *p*-refinement, as well as with increase of the temporal bases order, *M*, i.e., marching-on-in-degree.

In terms of the reported error of computation, the lowest achievable error with the proposed method in computed current is around 0.55%, which is consistent with the lowest errors reported in [6]. At the same time, the error of 0.56% is achieved very quickly with $N = 5$ in Fig. 7. The paper has presented results for the induced transient surface current densities as the most rigorous and critical representative of the solution accuracy in MoM-SIE modeling and assuming that the accuracy of far field computations is even better. Indeed, the presented solution with the 0.55% error in computed current yields 0.05% relative error in the RCS computation, which, in turn, is consistent with the lowest reported errors in [5].

Moreover, a major strength of the proposed method is *p*-convergence and ability for *p*-refinement, which should, in general, be combined with *h*-refinement, i.e., *hp*-refinement should be used. In that regard as well, this work is different when compared to all the existing MoM-TD methods in literature, which do not demonstrate such convergence of the solution with respect to *p*-refinement. This feature has been emphasized, for example, by a curve in Fig. 7 showing *p*-refinement of the model for the spatially non-refined mesh, which is quite unique and interesting: a highly accurate transient solution of a spherical scatterer modeled by only six elements of the fourth geometrical order and size $e \approx 1.34\lambda$ at $f_{\max 2}$ with eighth order spatial polynomial current approximation, resulting in only 768 unknowns.

The proposed method is a higher order and large-domain extension and advancement of the previously proposed and used low-order MoM-TD MOD method [19]–[26], and the importance of this advancement has been confirmed by the discussions and the results in the paper. In addition, this is the first time the accuracy is evaluated and convergence analyzed rigorously based on the relative error of the current (or far field, RCS, etc.) with respect to the analytical solution obtained by Mie series for MoM-TD MOD methods overall; there are no such reports in papers on low-order small-domain MOD methods and applications [19]–[26].

Future work includes extending the method to composite conducting-dielectric scattering structures.

References

[1] C. L. Bennett, Jr., "A technique for computing approximate electromagnetic impulse response of conducting bodies," Ph.D. dissertation, Purdue University, West Lafayette, Ind., 1968.

[2] S. M. Rao, *Time domain electromagnetics*, Academic Press, 1999.

[3] S. M. Rao and D. R. Wilton, "Transient scattering by conducting surfaces of arbitrary shape," *IEEE Transactions on Antennas and Propagation*, vol. 39, no. 1, pp. 56–61, January 1991.

[4] S. M. Rao and T. K. Sarkar, "An alternative version of the time-domain electric field integral equation for arbitrarily shaped conductors," *IEEE Transactions on Antennas and Propagation*, vol. 41, no. 6, pp. 831–834, June 1993.

[5] R. A. Wildman, G. Pisharody, D. S.Weile, S. Balasubramaniam, and E. Michielssen, "An Accurate Scheme for the Solution of the Time-Domain Integral Equations of Electromagnetics Using Higher Order Vector Bases and Bandlimited Extrapolation," *IEEE Transactions on Antennas and Propagation*, vol. 52. no. 11, pp. 2793–2984, November 2004.

[6] Y. Beghein, K. Cools, H. Bagci, and D. De Zutter, "A Space-Time Mixed Galerkin Marching-on-in-Time Scheme for the Time-Domain Combined Field Integral Equation," *IEEE Transactions on Antennas and Propagation*, vol. 61, no. 3, pp. 1228-1238, March 2013.

[7] A. J. Pray, Y. Beghein, N. V. Nair, K. Cools, H. Bagci, and B. Shanker, "A Stable Higher Order Space-Time Galerkin Scheme for Time Domain Integral Equations," ArXiv e-prints, arXiv:1401.2435, available on http://arxiv.org/abs/1401.2435

[8] S. M. Rao and T. K. Sarkar, "An efficient method to evaluate the time-domain scattering from arbitrarily shaped conducting bodies," *Microwave and Optical Technology Letters*, vol. 17, no. 5, pp. 321–325, April 1998.

[9] T. K. Sarkar, W. Lee, and S. M. Rao, "Analysis of transient scattering from composite arbitrarily shaped complex structures," *IEEE Transactions on Antennas and Propagation*, vol. 48, no. 10, pp. 1625–1634, October 2000.

[10] B. H. Jung and T. K. Sarkar, "An accurate and stable implicit solution for transient scattering and radiation from wire structures," *Microwave and Optical Technology Letters*, vol. 34, no. 5, pp. 354–359, September 2002.

[11] B. Shanker, A. A. Ergin, K. Aygun, and E. Michielssen, "Analysis of transient electromagnetic scattering from closed surfaces using a combined field integral equation," *IEEE Transactions on Antennas and Propagation*, vol. 48, no. 7, pp. 1064–1074, July 2000.

[12] B. Shanker, A. A. Ergin, M. Lu, E. Michielssen, "Fast analysis of transient electromagnetic scattering phenomena using the multilevel plane wave time domain algorithm," *IEEE Transactions on Antennas and Propagation*, vol. 51, no. 3, pp. 628–641, March 2003.

[13] G. Manara, A. Monorchio, and R. Reggiannini, "A space-time discretization criterion for a stable time-marching solution of the electric field integral equation," *IEEE Transactions on Antennas and Propagation*, vol. 45, no. 3, pp. 527–532, March 1997.

[14] B. Shanker, M. Lu, J. Yuan, and E. Michielssen, "Time domain integral equation analysis of scattering from composite bodies via exact evaluation of radiation fields," *IEEE Transactions on Antennas and Propagation*, vol. 57, no. 5, pp. 1506–1520, May 2009.

[15] Y. Shi, M. Y. Xia, R. S. Chen, E. Michielssen, and M. Lu, "Stable electric field TDIE solver via quasi-exact evaluation of MOT matrix elements," *IEEE Transactions on Antennas and Propagation*, vol. 59, no. 2, pp. 574–585, February 2011.

[16] A. E. Yilmaz, J. M. Jin, and E. Michielssen, "Time domain adaptive integral method for surface integral equations," *IEEE Transactions on Antennas and Propagation*, vol. 52, no. 10, pp. 2692– 2708, October 2004.

[17] H. Bağci, F. P. Andriulli, F. Vipiana, G. Vecchi, and E. Michielssen, "A well-conditioned integral-equation formulation for efficient transient analysis of electrically small microelectronic devices," *IEEE Transactions on Advance Packing*, vol. 33, no. 2, pp. 468–480, May 2010.

[18] T. K. Sarkar and J. Koh, "Generation of a wide-band electromagnetic response through a Laguerre expansion using early-time and low-frequency data," *IEEE Transactions on Antennas and Propagation*, vol. 50, no. 5, pp. 1408–1416, May 2002.

[19] Y. S. Chung, T. K. Sarkar, and B. H. Jung, "Solution of a time-domain magnetic-field integral equation for arbitrarily closed conducting bodies using an unconditionally stable methodology," *Microwave and Optical Technology Letters*, vol. 35, no. 6, pp. 493–499, December 2002.

[20] B. H. Jung, Y. S. Chung, and T. K. Sarkar, "Time-domain EFIE, MFIE, and CFIE formulations using Laguerre polynomials as temporal basis functions for the analysis of transient scattering from arbitrarily shaped conducting structures," *Progress in Electromagnetic Research*, vol. 39, pp. 1–45, 2003.

[21] Y. S. Chung, T. K. Sarkar, B. H. Jung, M. Salazar-Palma, Z. Ji, S. Jang, and K. Kim, "Solution of time domain electric field integral equation using the Laguerre polynomials," *IEEE Transactions on Antennas and Propagation*, vol. 52, no. 9, pp. 2319–2328, September 2004.

[22] B. H. Jung, T. K. Sarkar Y. S. Chung, M. Salazar-Palma, Z. Ji, S. Jang, and K. Kim, "Transient electromagnetic scattering from dielectric objects using the electric field integral equation with Laguerre polynomials as temporal basis functions," *IEEE Transactions on Antennas and Propagation*, vol. 52, no. 9, pp. 2329–2340, September 2004.

[23] Z. Ji, T. K. Sarkar, B. H. Jung, Y. S. Chung, M. Salazar-Palma, and M. Yuan, "A stable solution of time domain electric field integral equation for thin-wire antennas using the Laguerre polynomials," *IEEE Transactions on Antennas and Propagation*, vol. 52, no. 10, pp. 2641–2649, October 2004.

[24] B. H. Jung, T. K. Sarkar, S. W. Ting, Y. Zhang, Z. Mei, Z. Ji, M. Yuan, A. De, M. Salazar-Palma, and S. M. Rao, "Time and frequency domain solution of EM problems using integral equations and a hybrid methodology," Hoboken, New Jersey: *IEEE Press, John Wiley & Sons, Inc.*, 2010.

[25] Z. Ji, T. K. Sarkar, B. H. Jung, M. Yuan, and M. Salazar-Palma, "Solving time domain electric field integral equation without time variable," *IEEE Transactions on Antennas and Propagation*, vol. 54, no. 1, pp. 258–262, January 2006.

[26] Z. Mei, Y. Zhang, T. K. Sarkar, B. H. Jung, A. García-Lampérez, M. Salazar-Palma, "An improved marching-on-in-degree method using a new temporal basis," *IEEE Transactions on Antennas and Propagation*, vol. 59, no. 12, pp. 4643–4650, December 2011.

[27] S. M. Rao, D. R. Wilton, and A. W. Glisson, "Electromagnetic scattering by surfaces of arbitrary shape", *IEEE Transactions on Antennas and Propagation*, vol. AP-30, pp. 409–418, May 1982.

[28] B. M. Notaros, "Higher order frequency-domain computational electromagnetics," Special Issue on Large and Multiscale Computational Electromagnetics, *IEEE Transactions on Antennas and Propagation*, vol. 56, no. 8, pp. 2251−2276, August 2008.

[29] M. Đorđević and B. M. Notaroš, "Double higher order method of moments for surface integral equation modeling of metallic and dielectric antennas and scatterers," *IEEE Transactions on Antennas and Propagation*, vol. 52, no. 8, pp. 2118–2129, August 2004.

[30] M. J. Bluck and S. P. Walker, "Time-domain BIE analysis of large three-dimensional electromagnetic scattering problems," *IEEE Transactions on Antennas and Propagation*, vol. 45, no. 5, pp. 894–901, May 1997.

[31] M. D. Pocock, M. J. Bluck, and S. P. Walker, "Electromagnetic scattering from 3-D curved dielectric bodies using time-domain integral equations," *IEEE Transactions on Antennas and Propagation*, vol. 46, no. 8, pp. 1212–1219, August 1998.

[32] F. Valdés, M. Ghaffari-Miab, F. P. Andriulli, K. Cools, and E. Michielssen, "High-order Calderón preconditioned time domain integral equation solvers," *IEEE Transactions on Antennas and Propagation*, vol. 61, no. 5, pp. 2570–2588, May 2013.

[33] N. J. Šekeljić, M. M. Ilić and B. M. Notaroš, "Higher order time-domain finite element method for microwave device modeling with generalized hexahedral elements," *IEEE Transactions on Microwave Theory and Techniques*, vol. 61, no. 4, pp. 1425–1434, April 2013.

[34] J. A. Stratton, *Electromagnetic theory*, New York: McGraw-Hill, 1941.

[35] B. D. Popovic and B. M. Notaros, "Moment-method analysis of volume dielectric scatterers. Four independent entire-domain solutions: Is entire-domain philosophy a luxury or necessity in the method of moments?" (invited review paper), *International Journal of Microwave and Millimeter-Wave Computer-Aided Engineering*, vol. 6, (6), pp.454-473, November 1996.

[36] A. D. Poularikas, *The transforms and applications handbook*, Pistcataway, NJ: IEEE Press, 1963.

[37] E. M. Klopf, N. J. Šekeljić, M. M. Ilić and B. M. Notaroš, "Optimal modeling parameters for higher order MoM-SIE and FEM-MoM electromagnetic simulations," *IEEE Transactions on Antennas and Propagation*, vol. 60, no. 6, pp. 2790–2801, June 2012.

[38] B. H. Jung and T. K. Sarkar, "Time-domain CFIE for the analysis of transient scattering from arbitrarily shaped 3D conducting objects," *Microwave and Optical Technology Letters*, vol. 34, no. 4, pp. 289–296, August 2002.

[39] A. C. Woo, H. T. G. Wang, M. J. Schuh, and M. L. Sanders, "Benchmark radar targets for the validation of computational electromagnetics programs," *IEEE Antennas and Propagation Mag.*, vol. 35, no. 1, pp. 84–89, February 1993.

[40] A. Geranmayeh, "Time Domain Boundary Integral Equations Analysis", Ph.D. Dissertation, Vom Fachbereich Elektrotechnik und Informationstechnik der Technischen Universitat Darmstadt, Germany 2011.

[41] WIPL-D d.o.o. 2013. WIPL-D Pro v11.0. Available: http://www.wipl-d.com.

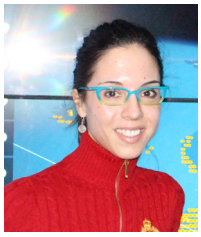

Nada J. Šekeljić (S'11) was born in Belgrade, Serbia, in 1984. She received the Dipl. Ing. (B.Sc.) degree in electrical engineering from the University of Belgrade, Belgrade, Serbia, in 2008, and is currently working toward the Ph.D. degree at Colorado State University, Fort Collins, Colorado.

Since 2008, she has been a Research Assistant with the Electromagnetics Laboratory, and Teaching Assistant with the Department of Electrical and Computer Engineering, Colorado State University. In summer 2013, she worked as signal integrity simulation intern at Hewlett-Packard, Fort Collins, CO. Her research interests are in computational and applied electromagnetics, and antenna design.

Milan M. Ilić (S'00–M'04) was born in Belgrade, Serbia, in 1970. He received the Dipl. Ing. and M.S. degrees in Electrical Engineering from the University of Belgrade, Serbia, in 1995 and 2000, respectively, and the Ph.D. degree from the University of Massachusetts Dartmouth, USA, in 2003.

He is currently an Associate Professor in the School of Electrical Engineering at the University of Belgrade and a postdoctoral Research Associate and Affiliated Faculty with the ECE department of the Colorado State University, USA. His research interests include computational electromagnetics, antennas, and microwave components and circuits.

Dr. Ilić was the recipient of the 2005 IEEE MTT-S Microwave Prize.

Branislav M. Notaroš (M'00-SM'03) was born in Zrenjanin, Yugoslavia, in 1965. He received the Dipl.Ing. (B.S.), M.S., and Ph.D. degrees in electrical engineering from the University of Belgrade, Belgrade, Yugoslavia, in 1988, 1992, and 1995, respectively.

From 1996 to 1999, he was an Assistant Professor in the School of Electrical Engineering at the University of Belgrade. He spent the 1998-1999 academic year as a Visiting Scholar at the University of Colorado at Boulder. He was an Assistant Professor, from 1999 to 2004, and Associate Professor, from 2004 to 2006, in the Department of Electrical and Computer Engineering at the University of Massachusetts Dartmouth. From 2006 to 2012, he was an Associate Professor in the Department of Electrical and Computer Engineering at Colorado State University, where he is currently a Professor and Director of Electromagnetics Laboratory. His research interests and activities are in computational electromagnetics, higher order numerical methods, antennas, scattering, microwaves, metamaterials, characterization of snow and rain, surface and radar precipitation measurements, RF design for MRI at ultra-high magnetic fields, and electromagnetics education. His publications include more than 150 journal and conference papers, and three workbooks in electromagnetics and in fundamentals of electrical engineering (basic circuits and fields). He is the author of textbooks *Electromagnetics* (Prentice Hall, 2010) and *MATLAB-Based Electromagnetics* (Prentice Hall, 2013), as well as the Electromagnetics Concept Inventory (EMCI).

Dr. Notaroš served as General Chair for the 11th International Workshop on Finite Elements for Microwave Engineering – FEM2012, June 4-6, 2012, Estes Park, Colorado, USA, and as Guest Editor of the Special Issue on Finite Elements for Microwave Engineering, Electromagnetics, Vol. 34, Issue 3-4, 2014. He was the recipient of the 2005 IEEE MTT-S Microwave Prize (best-paper award for IEEE Transactions on MTT), 1999 IEE Marconi Premium (best-paper award for IEE Proceedings on Microwaves, Antennas and Propagation), 1999 URSI Young Scientist Award, 2005 UMass Dartmouth Scholar of the Year Award, 2004 UMass Dartmouth College of Engineering Dean's Recognition Award, 1992 Belgrade Chamber of Industry and Commerce Best M.S. Thesis Award, 2009, 2010, 2011, and 2014 Colorado State University Electrical and Computer Engineering Excellence in Teaching Awards, 2010 Colorado State University College of Engineering George T. Abell Outstanding Teaching and Service Faculty Award, 2012 Colorado State University System Board of Governors Excellence in Undergraduate Teaching Award, 2014 Colorado State University Provost's N. Preston Davis Award for Instructional Innovation, 2012 IEEE Region 5 Outstanding Engineering Educator Award, 2014 Carnegie Foundation for the Advancement of Teaching Colorado Professor of the Year Award, and 2015 IEEE Undergraduate Teaching Award.